Inorg. Chem. **2003**, *42*, 6489–6496

Inorganic Chemistry

Article

EPR Spectroscopy of $[Fe_2O_2(5\text{-}Et_3\text{-}TPA)_2]^{3+}$: Electronic Origin of the Unique Spin-Hamiltonian Parameters of the $Fe_2^{III,IV}O_2$ Diamond Core

Andrew J. Skulan,[†] Melissa A. Hanson,[†] Hua-fen Hsu,[‡] Yanhong Dong,[‡] Lawrence Que, Jr.,*,[‡] and Edward I. Solomon*,[†]

Department of Chemistry, Stanford University, Stanford, California 94305, and Department of Chemistry and Center for Metals in Biocatalysis, University of Minnesota, 207 Pleasant Street SE, Minneapolis, Minnesota 55455

Received February 14, 2003

The electronic origins of the magnetic signatures of $[Fe_2O_2(5\text{-}Et_3\text{-}TPA)_2](ClO_4)_3$, where 5-Et$_3$-TPA = tris(5-ethyl-2-pyridylmethyl)amine, were investigated by density functional calculations. These signatures consist of a near-axial EPR spectrum, anisotropic superhyperfine broadening upon ^{17}O substitution in the Fe_2O_2 core, and an unusually large, positive zero-field splitting parameter, $D = 38 \pm 3$ cm^{-1}. Density functional calculations identify the anisotropic ^{17}O superhyperfine broadening to be due to a preponderance of oxo 2p density perpendicular to the plane of the Fe_2O_2 core in the three singly occupied molecular orbitals of the $S = {}^3/_2$ ground state. The near-axial **g**-matrix arises from $\Delta S = 0$ spin–orbit mixing between the singly and doubly occupied d_π orbitals of the iron d-manifold. The large D is due to $\Delta S = \pm 1$ spin–orbit mixing with low-lying d_π excited states. These experimental observables reflect the dominance of iron–oxo (rather than Fe–Fe) bonding in the Fe_2O_2 core, and define the low-lying valence orbitals responsible for reactivity.

1. Introduction

High-valent iron−oxo intermediates have been identified or implicated in a number of the oxygen activating binuclear non-heme iron enzymes.[1,2] Ribonucleotide reductase (RR) creates an $Fe_2^{III,IV}O_x$ (intermediate **X**) species during its reaction cycle[3−5] and methane monooxygenase (MMO) utilizes $Fe_2^{IV,IV}$-bis-μ-oxo (intermediate **Q**) for methane oxidation,[6] while a high-valent intermediate for Δ^9-desaturase (Δ9D) which has been postulated has not yet been trapped.[1,7,8] As the body of structural and spectroscopic data on these intermediates is not extensive, understanding the relationship between the known spectroscopic signatures of these molecules and their geometric and electronic origins is vital.

The only structurally characterized high-valent, binuclear non-heme iron complex is $[Fe_2O_2(5\text{-}Et_3\text{-}TPA)_2](ClO_4)_3$, where 5-Et$_3$-TPA = tris(5-ethyl-2-pyridylmethyl)amine.[9] This structure is of interest because it possesses the high oxidation state and structural features implicated in the reaction cycles of the binuclear non-heme iron enzymes and because it possesses reactivity paralleling the biological functions of these enzymes. It has been found to perform hydroxylation (monooxygenases), desaturation (desaturases), and radical formation (ribonucleotide reductases) with select organic substrates.[10,11] As shown in Chart 1, $[Fe_2O_2(5\text{-}Et_3\text{-}TPA)_2]$-$(ClO_4)_3$ has a bis-μ-oxo core supported by a tripodal, tetradentate capping ligand. This core has C_{2h} symmetry with alternating short (1.806 Å) and long (1.860 Å) Fe−O bonds,[9] consistent with the asymmetry (deviation from a D_{2h} rhombus) implied by EXAFS data from intermediate **Q**.[6] The

---

* Authors to whom correspondence should be addressed. E-mail: Edward.Solomon@stanford.edu (E.I.S.); que@chem.umn.edu (L.Q.).

[†] Stanford University.

[‡] University of Minnesota.

(1) Solomon, E. I.; Brunold, T. C.; Davis, M. I.; Kemsley, J. N.; Lee, S. K.; Lehnert, N.; Neese, F.; Skulan, A. J.; Yang, Y. S.; Zhou, J. *Chem. Rev.* **2000**, *100*, 235−349.

(2) Wallar, B. J.; Lipscomb, J. D. *Chem. Rev.* **1996**, *96*, 2625−2658.

(3) Edmondson, D. E.; Huynh, B. H. *Inorg. Chim. Acta* **1996**, *252*, 399−404.

(4) Que, L. *J. Chem. Soc., Dalton Trans.* **1997**, 3933−3940.

(5) Que, L.; Dong, Y. H. *Acc. Chem. Res.* **1996**, *29*, 190−196.

(6) Shu, L. J.; Nesheim, J. C.; Kauffmann, K.; Münck, E.; Lipscomb, J. D.; Que, L. *Science* **1997**, *275*, 515−518.

(7) Broadwater, J. A.; Achim, C.; Münck, E.; Fox, B. G. *Biochemistry* **1999**, *38*, 12197−12204.

(8) Broadwater, J. A.; Ai, J. Y.; Loehr, T. M.; Sanders-Loehr, J.; Fox, B. G. *Biochemistry* **1998**, *37*, 14664−14671.

(9) Hsu, H. F.; Dong, Y. H.; Shu, L. J.; Young, V. G.; Que, L. *J. Am. Chem. Soc.* **1999**, *121*, 5230−5237.

(10) Kim, C.; Dong, Y. H.; Que, L. *J. Am. Chem. Soc.* **1997**, *119*, 3635−3636.

(11) The reported reactivity studies were performed on the $[Fe_2O_2(TPA)_2]^{3+}$ complex.

10.1021/ic034170z CCC: $25.00

Chart 1. Core Geometry of $[Fe_2O_2(5\text{-}Et_3\text{-}TPA)_2]^{3+}$ Cation Showing the Molecular Coordinate System[a]

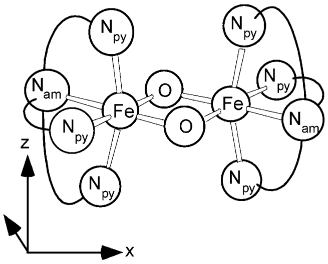

[a] The short Fe−O bonds are trans to the amine nitrogen donors, N_{am}.

magnetic signatures of $[Fe_2O_2(5\text{-}Et_3\text{-}TPA)_2]^{3+}$ have been previously reported to consist of a large positive zero-field splitting (ZFS), $D = 38 \pm 3$ cm^{-1}, a near-axial EPR spectrum with $g_{z'} = 2.01$, $g_{x'} = 2.08$, and $g_{y'} = 2.10$, and a single sharp Mössbauer doublet.[12−14] The origin of the large ZFS is of particular interest as iron complexes typically show $D < 3$ cm^{-1}.[1,15] These observations have led to the description of $[Fe_2O_2(5\text{-}Et_3\text{-}TPA)_2](ClO_4)_3$ as an $S = {}^3/_2$, class-III valence-delocalized $Fe_2^{III,IV}$ dimer generated from a pair of low-spin iron ions.[16] Initial density functional calculations (DFT) described the $S = {}^3/_2$ ground state in terms of two ferromagnetically coupled low-spin iron centers.[17]

Investigation of the vibrational (resonance Raman)[12,18] and excited state spectroscopies (low-temperature absorption and MCD and variable temperature−variable field (VTVH) MCD) of $[Fe_2O_2(5\text{-}Et_3\text{-}TPA)_2](ClO_4)_3$ and the relation of these results to the predictions of DFT calculations greatly expanded our understanding of the electronic structure of the diamond core.[12] DFT geometry optimizations indicated that the C_{2h} distortion of the Fe_2O_2 core was due to inequivalence of the sterically constrained nitrogen donors in the Fe_2O_2 plane (one tertiary amine and one pyridine ligand) (Chart 1). Normal coordinate analysis indicated that this C_{2h} distortion resulted in different stretching force constants for adjacent Fe−O bonds ($k_{str}(Fe{-}O_{long}) = 1.66$ and $k_{str}(Fe{-}O_{short}) = 2.72$ mdyn/Å) and a small (∼20%) difference in bond strength between adjacent Fe−O bonds. Valence delocalization to form a $S = {}^3/_2$ ground state is found to occur through three d_π superexchange pathways involving strong overlaps between p-orbitals on the bridging oxo ligands and d-orbitals on both iron atoms. No direct Fe−Fe overlap was identified, as anticipated by the 2.683 Å Fe−Fe separation. These orbitals were identified as key to the reactivity of this complex as they are oriented to overlap with the substrate C−H bonding orbital in a favorable trajectory for hydrogen atom abstraction.

This study utilizes spectroscopically verified DFT calculations[12] to determine the electronic origin of the magnetic signatures of $[Fe_2O_2(5\text{-}Et_3\text{-}TPA)_2](ClO_4)_3$. The nature of the singly occupied molecular orbitals (SOMOs) of the $S = {}^3/_2$ ground state are probed through anisotropic ^{17}O isotope superhyperfine broadening of the $g_{x'\text{eff}} = 3.9$ resonance of the EPR spectrum, while the specific spin−orbit interactions responsible for the near-axial **g**-matrix and **D**-tensor are identified from DFT calculations. These analyses are combined to correlate the magnetic coordinate system to the molecular frame (note coordinate system in Chart 1). This connection is important as it allows the relation of the polarizations of electronic transitions determined by VTVH MCD to the molecular coordinate system.[12] The molecular orbital analysis determines the origin of the large ZFS parameter, D. This study affirms and quantifies the nature of the singly occupied t_2 valence orbitals of the Fe_2O_2 diamond core that are key to its unique mixed-valent properties and reactivity.

2. Experimental Section

Sample Preparation. Green crystals of the complex $[Fe_2O_2(5\text{-}Et_3\text{-}TPA)_2](ClO_4)_3$, where 5-Et$_3$-TPA = tris(5-ethyl-2-pyridylmethyl)amine, were prepared as described previously.[13] The complex is thermally unstable at room temperature and was maintained below −20 °C. ***CAUTION!*** *The perchlorate salts in this study are all potentially explosive and should be handled with care.*

EPR Spectroscopy. A 0.6 mL portion of a stock solution of 0.5 mM $[Fe_2O_2(5\text{-}Et_3\text{-}TPA)_2](ClO_4)_3$ in dry CH_3CN was prepared at 238 K and divided into two parts. To one part was added an equal volume of a 50 mM solution of $NaClO_4$ in CH_3CN to which 2 μL $H_2{}^{16}O$ had been added. The other half was diluted likewise but with 2 μL of a $H_2{}^{17}O$/ $H_2{}^{16}O$ mixture (47:53 ratio). EPR spectra were collected at liquid helium temperatures on a Brüker E-500 spectrometer equipped with an Oxford Instruments ESR-10 liquid helium cryostat. The addition of $NaClO_4$ was observed to result in sharper EPR spectra. EPR spectra were baseline subtracted and simulated using XSophe (Brüker) using the spin-Hamiltonian,

$$\hat{H}_{spin} = \beta B \cdot \mathbf{g} \cdot \hat{\mathbf{S}} + \hat{\mathbf{S}} \cdot \mathbf{D} \cdot \hat{\mathbf{S}} + \hat{\mathbf{S}} \cdot \mathbf{A}[O] \cdot \hat{\mathbf{I}}[O] \qquad (1)$$

where β is the Bohr magneton, B is the magnetic field, **g** is the **g**-matrix, $\hat{\mathbf{S}}$ is the electron spin operator, **D** is the **D**-tensor, **A**[O] is the oxygen superhyperfine tensor, and $\hat{\mathbf{I}}$ is the nuclear spin operator of oxygen.

3. Results

3.1. EPR ^{17}O Isotope Effect. The X-band EPR spectra of $[Fe_2{}^aO_2(5\text{-}Et_3\text{-}TPA)_2](ClO_4)_3$, where $^aO = {}^{16}O$ or a 53:47 statistical mixture of ^{17}O:^{16}O, dissolved in CH_3CN are shown in Figure 1a. The same resonances are observed in both

---

(12) Skulan, A. J.; Hanson, M. A.; Hsu, H. F.; Que, L.; Solomon, E. I. *J. Am. Chem. Soc.* **2003**, *125*, 7344−7356.

(13) Dong, Y. H.; Fujii, H.; Hendrich, M. P.; Leising, R. A.; Pan, G. F.; Randall, C. R.; Wilkinson, E. C.; Zang, Y.; Que, L.; Fox, B. G.; Kauffmann, K.; Münck, E. *J. Am. Chem. Soc.* **1995**, *117*, 2778−2792.

(14) The primed coordinate system is defined by the effective **g**-tensor, with the z'-direction defined to be coincident with the distinct $g_{z'\text{eff}} = 2.01$ resonance, and $g_{x'\text{eff}} = 3.90$ and $g_{y'\text{eff}} = 4.45$. This is distinct from the molecular (unprimed) coordinate system of Chart 1 where z is perpendicular to the Fe2O2 plane and the x-axis coincides with the Fe−Fe vector.

(15) Two notable exceptions are the Fe(IV)═O(cyclam-acetato)$^+$ complex, $D = 23$ cm^{-1} (Grapperhaus et al. *Inorg. Chem.* **2000**, 39, 5306−5317), and Compound II of Horseradish Peroxidase, $D = 32$ cm^{-1} (Schultz, C. E., et al. *Biochemistry* **1984**, *23*, 4743−4754).

(16) "Class III valence-delocalized" means the two metal centers are elctronically equivalent (Robin, M. B.; Day, P. *Adv. Inorg. Chem. Radiochem.* **1967**, *10*, 247−403). This is consistent with the C_{2h} Fe_2O_2 core symmetry as the two metal atoms are related by the C_2 rotation element.

(17) Ghosh, A.; Almlof, J.; Que, L. *Angew. Chem., Int. Ed. Engl.* **1996**, *35*, 770−772.

(18) Wilkinson, E. C.; Dong, Y. H.; Zang, Y.; Fujii, H.; Fraczkiewicz, R.; Fraczkiewicz, G.; Czernuszewicz, R. S.; Que, L. *J. Am. Chem. Soc.* **1998**, *120*, 955−962.

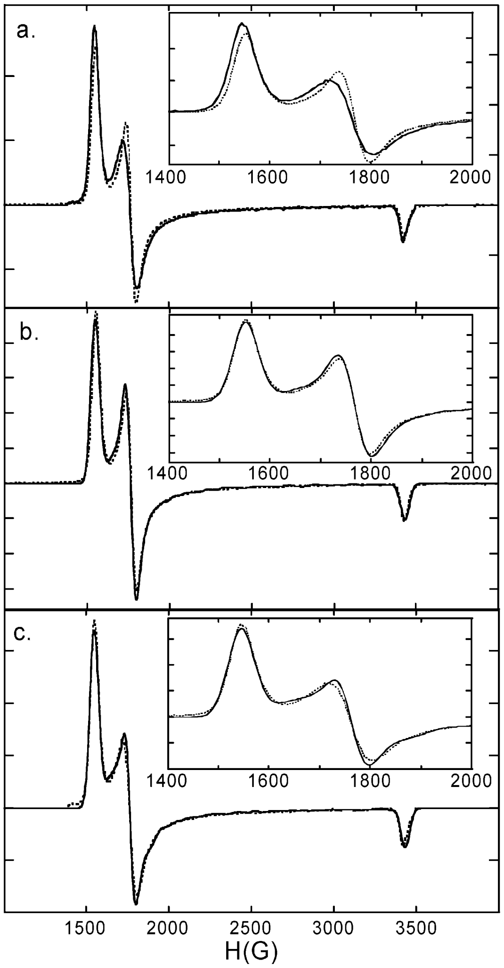

Figure 1. ^{16}O and 53:47 ^{17}O:^{16}O EPR spectra and their simulations. All spectra are calculated using $g_{x',y',z'} = (2.073, 2.092, 2.013)$, $D = 37.9$ cm^{-1}, $E/D = 0.0041$, $W_{x',y',z'} = (55, 62, 30)$, $\nu(^{16}O) = 9.627080$ MHz, $\nu(^{17}O) = 9.625130$ MHz, $T = 20$ K. (a) ^{16}O (dashed) and 53:47 ^{17}O:^{16}O (solid) EPR spectra. Inset: magnified 1400−2000 G region. (b) ^{16}O EPR spectrum (solid) and simulated ^{16}O spectrum (dashed). Inset: magnified 1400−2000 G region. (c) ^{17}O EPR spectrum (solid) and simulated ^{17}O spectrum (dashed). $A[O]_{x',y',z'} = (33, 2.9, 1.1)$. Inset: magnified 1400−2000 G region.

spectra (at $g_{\mathrm{eff}} = 2.01$, 3.90, and 4.45), but with significant broadening present in only the $g_{x'\mathrm{eff}} = 3.90$ resonance (Figure 1a). The presence of anisotropic broadening upon oxygen isotope substitution indicates unequal distribution of the singly occupied molecular orbitals' (SOMOs') oxygen-based spin density among the directionally distinct 2p orbitals. Broadening in only the x' direction indicates that the magnetic x'-axis contains a preponderance of the oxo spin density in the SOMOs. This observation was quantified via EPR simulations. The ^{16}O spectrum was well simulated ($R^2 = 0.97$) by $g_{x'} = 2.073$, $g_{y'} = 2.092$, $g_{z'} = 2.013$, $D = 37.9$ cm^{-1}, $E/D = 0.0041$, $W_{x'} = 55$ G, $W_{y'} = 62$ G, and $W_{z'} = 30$ G[19] (Figure 1b).[20] These parameters were used to simulate the ^{17}O spectrum with the addition of the oxygen superhyperfine tensor which was fit as $|A[O]_{x'}| = 33 \times 10^{-4}$ cm^{-1}, $|A[O]_{y'}| = 2.9 \times 10^{-4}$ cm^{-1}, and $|A[O]_{z'}| = 1.1 \times 10^{-4}$ cm^{-1} (Figure 1c).[21] The oxygen superhyperfine tensor elements fit the experimental data well to tolerances of $\pm 8 \times 10^{-4}$ cm^{-1}. The **g**-matrix, **D**-tensor, and **A**[O]-tensor were coaxial in the simulations. The axial direction of the oxygen superhyperfine tensor will be correlated with the orbital compositions of SOMOs obtained from density functional calculations to orient the magnetic coordinate system (x', y', z') relative to the molecular coordinate system (x, y, z) of Chart 1.

Table 1. Percentage Contributions to Molecular Orbitals of Geometry Optimized Model. Only Majority Spin−Orbitals Are Shown as the Corresponding Minority Spin−Orbital's Occupations Differ by <10%. Dashed Lines Separate Doubly Occupied "t_2" (bottom), Singly Occupied "t_2*" (middle) and Unoccupied "e" (top) Orbitals.

	MO distribution			
MO label	% Fe	% oxo	% NH_3	major orbital contributions
$xy(+)$	59	24	16	55% Fe $d_{x^2-y^2}$, 23% Op_x
$xy(-)$	60	27	13	59% Fe $d_{x^2-y^2}$, 1% Fe d_{xy}, 26% Op_y
$z^2(-)$	64	8	27	61% $Fed_z{}^2$, 7% Op_x, 1% Op_y
$z^2(+)$	64	8	27	52% $Fed_z{}^2$, 8% Fe d_{xy}, 8% Op_y
$xz(-)$	60	31	9	60% Fe d_{xz}, 31% Op_z
$yz(+)$	61	38	1	61% Fe d_{yz}, 2% Fed_{xz}, 38% Op_z
$x^2-y^2(+)$	73	18	8	62% Fe d_{xy}, 11% $Fed_z{}^2$, 18% Op_y
$x^2-y^2(-)$	77	17	5	76% Fe d_{xy}, 9% Op_x, 9% Op_y
$xz(+)$	89	1	10	87% Fe d_{xz}
$yz(-)$	97	1	2	97% Fe d_{yz}

3.2. Electronic Structure Calculations. The DFT calculations used in this study are described in detail elsewhere.[12] Relevant results are presented here for the analysis in this paper.

Spin-unrestricted calculations were performed using ADF 2.01[22,23] with basis set IV and the BP86 functional. The computational model was $Fe_2O_2(NH_3)_8$, a truncated version of the molecule under investigation where the pyridine and tertiary amine ligands have been replaced with ammonia.[12] Table 1 and Figure 2 show the part of the molecular orbital energy level diagram relevant to this study. The d-orbital manifold is split into three regions: three doubly (both majority and minority spin) occupied "t_2" orbitals, three singly (majority spin) occupied "t_2*" (Figure 3) orbitals, and four unoccupied "e" orbitals. This ligand field splitting between the t_2/t_2*[24] and e sets of orbitals is typical of a distorted octahedral geometry for the individual iron atoms. Note that the labels "t_2" and "t_2*" differentiate the lower energy, doubly occupied orbitals (t_2) from the higher energy, singly occupied orbitals (t_2*) which are most strongly antibonding with the oxo bridges. The four highest energy t_2/t_2* orbitals have π* overlap with the bridging oxo ligands, while for the remaining two these bonding interactions are

---

(19) Differences in spectral line widths could be simulated by addition of a nitrogen superhyperfine coupling term to the spin-Hamiltonian, although this was just as easily accounted for by field-dependent broadening, meaning that little information regarding the nature of nitrogen contributions to the SOMOs could be extracted from the data. For this reason, the spectra were fit using different line widths for each spectral resonance.

(20) Resonance positions in the EPR spectrum depend upon both the **g**-matrix and **D**-tensor. This leads to a range of simulations which correlate well with the experimental spectrum. Elements of the **g**-matrix can vary by ±0.01, while **D**-tensor elements can vary by 0.05 cm^{-1}.

(21) EPR spectra are insensitive to the sign of superhyperfine tensor values.

(22) Baerends, E. J.; Ellis, D. E.; Ros, P. *J. Chem. Phys.* **1973**, *2*, 42.

(23) te Velde, G.; Barerends, E. J. *Int. J. Comput. Phys.* **1992**, *99*, 84.

(24) The notation "t_2/t_2*" indicates that we are considering the members of both the t_2 and t_2* sets of orbitals. Similarly "t_2/t_2* → e" indicates a transition from a member of either the t_2 or t_2* sets of orbitals to a member of the e set of orbitals.

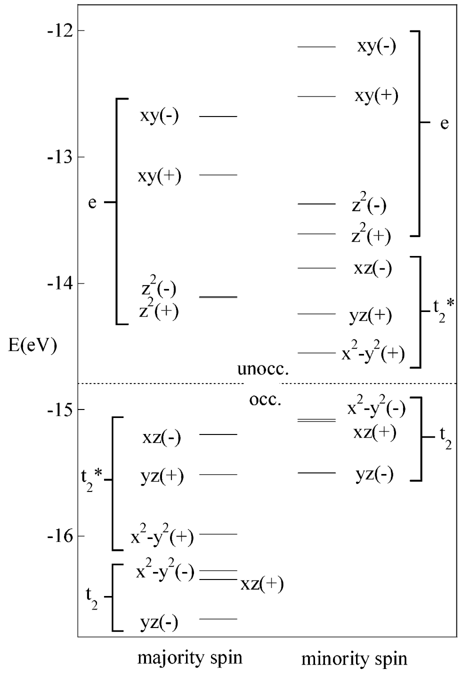

Figure 2. Energy level diagram obtained from a DFT calculation on $Fe_2O_2(NH_3)_6$ showing the d-manifold energy splittings.

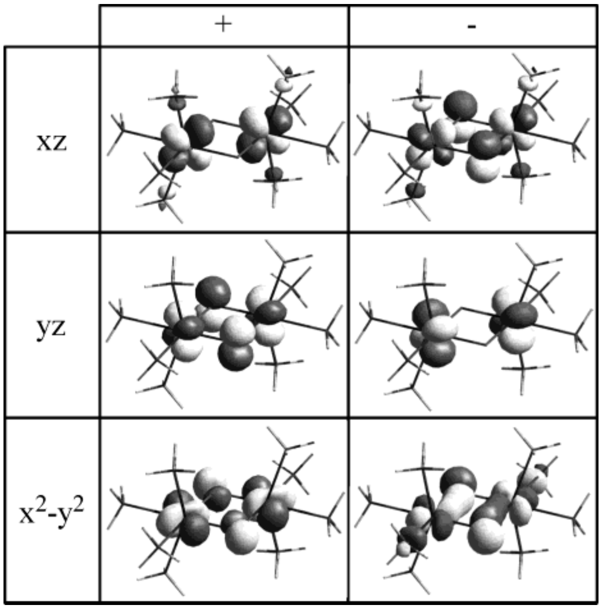

Figure 3. The t_2 and t_2* orbitals. $xz(-)$, $yz(+)$, and $x^2-y^2(+)$ are the singly occupied t_2* while $xz(+)$, $yz(-)$, and $x^2-y^2(-)$ are the doubly occupied t_2.

symmetry forbidden. The four "e" orbitals, $z^2(+)$, $z^2(-)$, $xy(+)$, and $xy(-)$,[25] have σ* overlap with the ligands (xy is in the e set of orbitals as the molecular coordinate system is oriented with the x-axis bisecting the O−Fe−O angle (Chart 1)). The $xy(\pm)$ orbitals are at a higher energy than the $z^2(\pm)$ orbitals due to better σ-overlap with the strong oxo donor ligands.

4. Analysis

Spin Hamiltonian Parameters. Experiment has identified a $S = {}^3/_2$ molecular ground state for $[Fe_2O_2(5\text{-}Et_3\text{-}TPA)_2](ClO_4)_3$, possessing a near-axial positive **D**-tensor ($E/D = 0.05$) with a large zero-field splitting.[13] As the molecular symmetry identified from the crystal structure is rhombic (C_{2h}), the unique direction of the **D**-tensor may be aligned along any of three perpendicular axes of the molecular coordinate system where x = Fe−Fe, $y \approx$ O−O, and z = perpendicular to the Fe_2O_2 core (Chart 1). Determining this orientation is of importance as this allows the polarizations of transitions from VTVH MCD to be related to specific molecular orbitals and helps evaluate how well the calculation reproduces the molecular electronic structure. The density functional calculation has identified $xz(-)$, $yz(+)$, and $x^2-y^2(+)$ (Figure 2 and Figure 3) as the singly occupied molecular orbitals. Their oxo orbital contributions will be used to define the direction of greatest superhyperfine broadening (the x' direction), while their spin−orbit coupling with electronic excited states will determine the orientation of the **g**-matrix (the z'-axis) in the molecular frame. This analysis of the DFT wave function will then be extended to determine the MO origin of the large ZFS of $[Fe_2O_2(5\text{-}Et_3\text{-}TPA)_2](ClO_4)_3$.

4.1. ^{17}O Superhyperfine Broadening. The superhyperfine broadening of features in the EPR spectrum in Figure 1a upon isotopic substitution are due to a number of interactions between ligand nuclear spins and unpaired electron spins.[26,27] Upon substituting ^{17}O for ^{16}O in the Fe_2O_2 core, the nuclear spin changes from $I_N(^{16}O) = 0$ to $I_N(^{17}O) = {}^5/_2$. This introduces anisotropic spin dipolar coupling due to the oxo 2p orbital character and isotropic Fermi contact interactions associated with the oxo 2s orbital contribution. This is expressed, to first order, by

$$A^{L}(j) = \sum_{xz(-),yz(+),x^2-y^2(+)} \frac{g_e\beta_e g_n\beta_n}{\langle r_{O(2p)}{}^3\rangle} \times \frac{2}{5}(3\cos^2\theta - 1)|c(O(2p_{i,j}))|^2 + \frac{8\pi}{3} g_e\beta_e g_n\beta_n |c(O(2s))|^2 \quad (2)$$

where A^L is the superhyperfine coupling tensor of atom L, j indicates the Cartesian directions ($j = x, y, z$), the summation is over the SOMOs, g_e is the free electron g-value, g_n is the nuclear g-value, β_e is the electronic Bohr magneton, β_n is the nuclear Bohr magneton, $\langle r_{O(2p)}\rangle$ is the expectation value of the radial component of the oxygen 2p wave function, θ is the angle between the axis direction j and the orientation of the oxygen p-orbital, $|c(O(2p_{i,j}))|^2$ is the unpaired spin density of the oxygen p_j-orbital in molecular orbital i, and $|c(O(2s))|^2$ is the unpaired spin density in the oxygen

---

[25] The (+) and (−) notation refers to relative phases of orbitals in the (x,y,z) molecular coordinate system. For the Fe-based orbitals, (+) also indicates gerade inversion symmetry, while (−) is ungerade.

[26] Solomon, E. I. *Comments Inorg. Chem.* **1984**, *3*, 225−320.

[27] Bencini, A.; Gatteschi, D. In *Inorganic Electronic Structure and Spectroscopy*; Solomon, E. I., Lever, A. B. P., Eds.; John Wiley & Sons: New York, 1999; Vol. 1, pp 93−160.

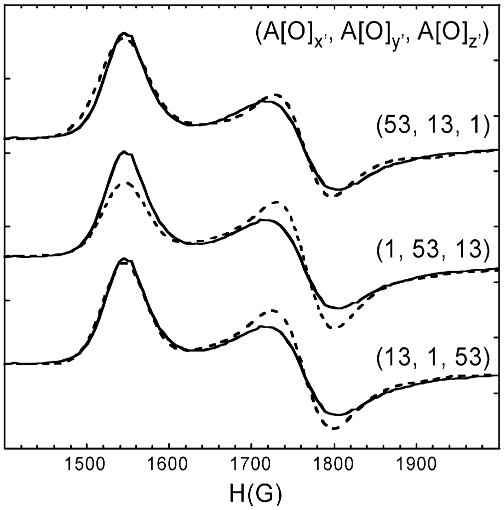

Figure 4. 1400−2000 G regions of the ^{17}O EPR spectrum (solid) and simulated ^{17}O spectrum (dashed) for a range of **A**[O] tensor orientations using the values determined from DFT calculations. All simulations use $g_{x',y',z'} = (2.073, 2.092, 2.013)$, $D = 37.9$ cm^{-1}, $E/D = 0.0041$, $W_{x',y',z'} = (55, 62, 30)$, $\nu(^{16}O) = 9.627080$ MHz, $\nu(^{17}O) = 9.625130$ MHz, $T = 20$ K. Respective values for ($A[O]_{x'}$, $A[O]_{y'}$, $A[O]_{z'}$) are shown in the figure.

s-orbital. Using the coordinate system of Chart 1 and eq 2, the calculated oxygen superhyperfine tensor is $A[O]_x = 13 \times 10^{-4}$ cm^{-1}, $A[O]_y = -0.9 \times 10^{-4}$ cm^{-1}, and $A[O]_z = -53 \times 10^{-4}$ cm^{-1} where *x*, *y*, *z* are in the molecular frame.[28]

The isotopic mixture of the "^{17}O" sample is 53:47 ^{17}O:^{16}O, which results in a statistical mixture of binuclear cores: 22% $Fe_2{}^{16}O_2L_2$, 50% $Fe_2{}^{16}O^{17}OL_2$, and 28% $Fe_2{}^{17}O_2L_2$. This mixture was simulated as a weighted sum of the three spectra. Simulations of the mixed-isotope EPR spectrum were performed with the three calculated oxygen superhyperfine tensor values, $A[O]_x$, $A[O]_y$, and $A[O]_z$, being permuted among the three magnetic tensor directions, $A[O]_{x'}$, $A[O]_{y'}$, and $A[O]_{z'}$. The three limiting cases are shown in Figure 4, with the largest broadening along each of the primed axis directions (x', y', and z'). The best fit is achieved when $A[O]_{x'}$, corresponding to the $g_{\text{eff}} = 3.9$ direction, is large and the other two are smaller (Figure 4, top). If $A[O]_{y'}$ is largest, then the positive peaks of the $g_{\text{eff}} = 4.45$ and the $g_{\text{eff}} = 3.9$ features are of similar height (Figure 4, middle), while if $A[O]_{z'}$ is largest, then the $g_{\text{eff}} = 3.9$ broadening is significantly underestimated (Figure 4, bottom), neither of which reproduces the experimentally observed behavior.

^{17}O superhyperfine broadening is predominantly observed in the $g_{x'}$ resonance of the EPR spectrum. DFT calculations predict that the principal direction of the oxygen superhyperfine tensor is the *z*-direction (normal to the Fe_2O_2 plane in Chart 1) of the molecular coordinate system. This leads to the conclusion that the x'-direction of the magnetic coordinate system corresponds to the *z*-direction of the molecular coordinate system. The orientation of the y' and z' magnetic directions relative to the *x* and *y* molecular axes cannot be determined from the superhyperfine broadening data as the simulated spectrum undergoes only minor changes upon swapping the $A[O]_x$ and $A[O]_y$ values (Table 2, Figure 4, top, and Supporting Information).

The calculated values and the resulting spectrum (with $A[O]_{x'}$ largest) are similar to those of the *A*[O] floated fit (Table 2, columns 2 and 3), although the magnitudes of $A[O]_z$ and $A[O]_y$ were overestimated by calculation. The $t_2 \rightarrow t_2^*$ transition energies calculated via BP86 DFT are also overestimated by 40% relative to the MCD spectrum.[12,29] This suggests that the BP86 DFT calculation overestimates the interaction between the iron d- and oxo p-orbitals which is manifest in an overestimation of the covalency (i.e., the oxo character) and energy splitting of the three singly occupied valence orbitals.[30] Decreasing the calculated oxygen superhyperfine tensor by 40% (to $A[O]_{x'} = -32 \times 10^{-4}$ cm^{-1}, $A[O]_{y'} = -0.5 \times 10^{-4}$ cm^{-1}, and $A[O]_{z'} = 8 \times 10^{-4}$ cm^{-1}; *vide infra* for final orientation of magnetic and molecular coordinate systems) generates a simulation which is nearly indistinguishable from the empirical ^{17}O *A*[O] fit ($A[O]_{x'} = 33 \times 10^{-4}$ cm^{-1}, $A[O]_{y'} = 2.9 \times 10^{-4}$ cm^{-1}, and $A[O]_{z'} = 1.1 \times 10^{-4}$ cm^{-1}) (Supporting Information).

4.2. Direction and Orbital Origins of g-Matrix and Zero Field Splitting Tensor. 4.2.1 g-Matrix. The **g**-matrix is observed to be near-axial, with one distinct ($g_{z'} = 2.01$) and two similar values ($g_{x'} = 2.07$ and $g_{y'} = 2.09$). Deviations from the free-electron *g*-value ($g = 2.0023$) are due to $\Delta S = 0$ spin−orbit coupling of excited states into the ground state. This can be calculated from eq 3,[31]

$$\Delta g_{pq} = -\frac{1}{S_a}\sum_b \Delta_b^{-1}\delta_{S_aS_b} \times \Big\{\langle aS_aS_a|\sum_i l_p(i)|bS_bS_b\rangle\langle bS_bS_b|\sum_{A,i}\xi(r_{iA})l_q(i)s_0(i)|aS_aS_a\rangle + \langle aS_aS_a|\sum_{A,i}\xi(r_{iA})l_q(i)s_0(i)|bS_bS_b\rangle\langle bS_bS_b|\sum_i l_p(i)|aS_aS_a\rangle\Big\} \quad (3)$$

where Δg_{pq} is the deviation from $g = 2.0023$, S_a is the spin of the system, Δ_b is the energy difference between the ground

---

[28] The calculated $A[O]_y$ tensor direction is aligned with the O−O vector, while C_{2h} symmetry requires the $A[O]_z$ direction to coincide with the molecular *z*-direction. While not identical to the molecular coordinate system, the labels $A[O]_x$ and $A[O]_y$ are used for clarity of discussion.

[29] The $t_2 \rightarrow t_2^*$ electronic transition energies are overestimated by calculation. The calculated value is 43% greater than the experimental for $yz(-) \rightarrow yz(+)$, while for $xz(+) \rightarrow xz(-)$ the calculated energy is 39% greater than experiment.

[30] The ligand electron density present in a metal-based MO, c_b^2, is a function of the interaction matrix element between the metal and ligand orbital, H_{ab}, and the energy splitting between the non-interacting component atomic orbitals, ΔE: $c_b^2 = H_{ab}^2/\Delta E^2$. The energy destabilization of the metal orbital due to this metal−ligand covalent interaction, ΔW, is $\Delta W = H_{ab}^2/\Delta E$. Hence, c_b^2 is proportional to ΔW. Covalency scaling was performed by decreasing the coefficient of the oxo orbital contribution to the d-manifold by 40%, i.e., $(c_{\text{oxo covalency scaled}})^2 = 0.6(c_{\text{oxo bp86 calcd}})^2$, and proportionally decreasing the energy splitting between the $yz(-)$ and the other five t_2 and t_2^* orbitals by a factor of 0.6. $yz(-)$ approximates the nonbonding limit as it is 97% Fe; e.g., $xz(-)$ (Table 3) changes from 60% Fe and 31% oxo to 76% Fe and 19% oxo and ΔW (the energy difference between $yz(-)$ and $xz(-)$) decreases from 11930 to 7160 cm^{-1} upon covalency scaling. This scaling is supported by the overestimation of the $t_2 \rightarrow t_2^*$ transition energies, the poor correlation between calculated and experimental **g**-matrices prior to scaling, and overestimation of the oxygen superhyperfine tensor, in the unscaled BP86 DFT calculation. Each of these correlations improves upon covalency scaling.

[31] Neese, F.; Solomon, E. I. *Inorg. Chem.* **1998**, *37*, 6568−6582.

Table 2. Quality of Fit for ^{16}O and ^{17}O Simulation Parameter Sets

parameter	^{16}O best fit	^{17}O best fit	^{17}O (53,13,1)	^{17}O (13,53,1)	^{17}O (1,13,53)	^{17}O (1,53,13)	^{17}O (53,1,13)	^{17}O (13,1,53)
$A[\mathrm{O}]_{x'}$ [a]	0	33	53	13	1	1	53	13
$A[\mathrm{O}]_{y'}$ [a]	0	2.9	13	53	13	53	1	1
$A[\mathrm{O}]_{z'}$ [a]	0	1.1	1	1	53	13	13	53
R^2 [b]	0.98	0.99	0.98	0.93	0.90	0.90	0.98	0.96

[a] Units: A[O] in 10^{-4} cm^{-1}. [b] R^2 is calculated over the range 1600−2000 G, under which the $g_{\mathrm{eff}} = 3.90$ resonance is found. The R^2 value for the correlation between the ^{16}O and ^{17}O experimental spectra was 0.93.

Table 3. Comparison of Experimental and Calculated g-Values[a]

axis	expt	full DFT calcn	60% covalency
g_x	2.01	1.99	1.99
g_y	2.07	1.95	2.08
g_z	2.09	2.03	2.09

[a] The "60% covalency" calculation decreased the covalency and splitting of t_2/t_2^* orbital pairs by 60%[30] relative to the full BP86 DFT calculation.

state "a" and excited state "b", $l_{\mathrm{p}}(i)$ is the one-electron angular momentum operator on electron i along Cartesian direction p, $\xi_{\mathrm{A}}(i)$ is the spin−orbit radial operator ($\xi(i) = (2.67 \times 10^{-5})Z_{\mathrm{eff}}r_i^{-3}$), $|aS_aS_a\rangle$ represents the ground state wave function and $|bS_bS_b\rangle$ represents the excited state wave function. A number of simplifications were made in application of this expression to the density functional generated wave functions for this molecule. $\xi_A(i)$ is approximated by the average of the Fe^{3+} and Fe^{4+} free ion SOC constants, 490 cm^{-1}. This value is an order of magnitude greater than the SOC value of oxygen, making it a reasonable approximation to consider only the iron contribution when calculating spin−orbit mixing with excited states. The angular momentum operator is executed using the individual iron atoms as the rotational origins, generating a pair of identical **g**-matrices that are centered upon the two iron nuclei. These two tensors are coupled to find the total molecular **g**-matrix.

Only excited states of the same spin as the ground state, $^4\Gamma$, and differing by a single one-electron transition contribute to the **g**-matrix. Contributions from transitions from doubly occupied to singly occupied molecular orbitals result in a positive contribution to Δg_{pq}. The inverse proportionality of the transition energy and the dependence upon the iron spin density in both the donor and acceptor orbitals determine that only transitions from $t_2 \rightarrow t_2^*$ and oxo $\rightarrow t_2^*$ orbitals will significantly contribute to the positive deviations from $g = 2.0023$. Conversely, transitions from the singly occupied to unoccupied molecular orbitals make a negative contribution to Δg_{pq}. Transition energy and iron covalency limit major negative contributors to Δg_{pq} to those arising from spin−orbit coupling between the t_2^* and e manifolds. $\Delta S = 0$ transitions from doubly occupied to unoccupied molecular orbitals need not be considered as any contributions from the mixing of an excited state involving a majority spin transition will be negated by a contribution from excited state mixing of the corresponding minority spin−orbital which will have the same magnitude (differences between the majority and minority spin−orbitals due to spin polarization notwithstanding) but opposite signs. Each of the experimental g-values is greater than 2.0023, indicating that the contribution from doubly occupied into singly occupied orbitals outweighs those from singly occupied into the unoccupied orbitals. It is of interest to note that the two contributions nearly cancel each other in the case of $g_{z'}$ ($\Delta g_{z'\mathrm{expt}} = 0.007$).

The **g**-matrix predicted by the density functional generated wave function is $g_x = 1.99$, $g_y = 1.95$, $g_z = 2.03$. It does not reproduce the experimental values: 2.01, 2.07, and 2.09. The three calculated g-values are equally spaced, suggesting a highly rhombic electronic environment, not the near-axial orientation observed experimentally. The predicted value of Δg_x and Δg_y is of the wrong sign (all experimental deviations from $g_i = 2.0023$ are positive), indicating that the $t_2^* \rightarrow$ e contributions disproportionally outweigh those from oxo $\rightarrow t_2^*$ and $t_2 \rightarrow t_2^*$. The calculated wave function may be overestimating the energy splitting between the t_2^* and the t_2 and oxo-based orbitals or underestimating the $t_2^* \rightarrow$ e splitting.

It has been observed from the analysis of the ^{17}O superhyperfine broadening in the EPR spectrum (see section 4.1) and from the low-energy MCD transitions[12,29] that the covalencies and energies of the SOMOs are overstated by the calculation. This will also overly destabilize the t_2^* antibonding orbitals, overestimating the deviation of the t_2 manifold from the nonbonding energy. Decreasing the covalency (the square of the coefficient of the ligand atomic orbitals in a molecular orbital, c_{l}^2) by 40%[30] (based on the analysis of ^{17}O superhyperfine broadening) and proportionally decreasing the energy splitting between the t_2 and t_2^* sets of orbitals by 40% (based upon calculated versus experimental $t_2 \rightarrow t_2^*$ transition energies[12]) gives $g_x = 1.99$, $g_y = 2.08$, $g_z = 2.09$.[32,33] The experimental and calculated g-values are compared in Table 3. The increases in the Δg elements upon decreasing the covalency are due to the cumulative effects of lowering the negative contribution from $t_2^* \rightarrow$ e mixing and increasing the oxo $\rightarrow t_2^*$ and $t_2 \rightarrow t_2^*$ interaction due to the $\Delta g \propto \Delta^{-1}$ dependence of eq 3. The g-values generated using the experimentally calibrated calculation reproduce the experimental g-values well ($g_{z'} < g_{x'} \approx g_{y'}$) with $g_x < g_y \approx g_z$.

---

(32) The calculated **g**-matrix is rotated by 2° toward the short Fe−O bond in the Fe$_2$O$_2$ plane, while C_{2h} symmetry requires the g_z-direction to coincide with the molecular z-direction. While not identical to the molecular coordinate system, the labels g_x and g_y are used for clarity of discussion.

(33) g_x is less than 2.0023 in both full and covalency-scaled calculations as the calculated splitting of the d-manifold incorrectly predicts that the negative contribution from $t_2^* \rightarrow$ e mixing outweighs the positive contribution of $t_2 \rightarrow t_2^*$ mixing. The difference between calculated and experimental g_x values is small and is due to the assumptions described above for calculating the **g**-matrix.

Table 4. Relationship between the Magnetic and Molecular Coordinate Systems and the Source of This Correlation

magnetic coord syst	molecular coord syst	experimental source
x'	z	^{17}O EPR hyperfine broadening
y'	y	
z'	x	EPR **g**-matrix/ZFS tensor

This calculation has identified the orientation of the unique axis of the near-axial **g**-matrix (and the magnetic coordinate system in which it is located). It is observed experimentally that $g_{z'} = 2.01$ is distinct from $g_{y'}$ and $g_{x'}$, while the above **g**-matrix calculation identifies the molecular x-axis, which points along the metal−metal vector, as magnetically distinct ($z' = x$). ^{17}O EPR superhyperfine broadening (see section 4.1) has been previously shown to have $x' = z$, uniquely determining the orientations of the two axes relative to each other; $z' = x$, $y' = y$, and $x' = z$ (Table 4). This correspondence of magnetic and molecular coordinates allows the polarization of electronic transitions determined via simulations of VTVH MCD saturation behavior to be mapped onto the molecular structure.

4.2.2. D-Tensor. The zero-field splitting has been measured to be 35 ± 15 cm^{-1} ($E/D = \sim 0.05$) by temperature-dependent EPR and Mössbauer spectroscopies[13] and 38 ± 3 cm^{-1} from simulations of VTVH MCD data.[12] This value is unusually large in comparison to mononuclear ferric iron molecules which display the range $-5 \le D \le 5$ cm^{-1}, although initial reports of monomeric Fe(IV) ZFS show larger values for D.[15] This splitting of the electronic ground state's spin states can be due to spin−orbit coupling of electronic excited states of the same spin ($S_{\text{e.s.}} = S_{\text{g.s.}}$) into the ground state (the same mechanism as for **g**-matrix deviations from $g = 2.0023$) or from states differing by one spin flip ($S_{\text{e.s.}} = S_{\text{g.s.}} \pm 1$). It is common to consider only the $\Delta S = 0$ **D**-tensor, $D^{(0)}$, as given by eq 4:[31]

$$D_{pq}^{(0)} = -\frac{1}{S_a^{\,2}}\sum_b \Delta_b^{-1}\delta_{S_aS_b}\langle aS_aS_a|\sum_{A,i}\xi(r_{iA})l_{A,p}(i)s_0(i)|bS_bS_b\rangle \times \langle bS_bS_b|\sum_{A,i}\xi(r_{iA})l_{A,q}(i)s_0(i)|aS_aS_a\rangle \quad (4)$$

The variables have the same definitions as in eq 3, and the same simplifications are used. The spin-Hamiltonian parameter, D, equals $D_{zz} - {}^1/_2(D_{xx} + D_{yy})$ in a diagonalized **D**-tensor. Applying this to the covalency-scaled DFT wave function[30] results in $D = 10.6$ cm^{-1} and $E/D = 0.034$. The small calculated rhombicity is consistent with experiment, while the magnitude of D is four times smaller than the experimental value, indicating that there must be additional contributions to the ZFS. The other possible contributions to D are from $\Delta S = \pm 1$ excited states that are given by[31]

$$D_{pq}^{(+1)} = -\frac{1}{(S_a+1)(2S_a+1)} \times \sum_b \Delta_b^{-1}\delta_{S_bS_a+1}\langle aS_aS_a|\sum_{A,i}\xi(r_{iA})l_{A,p}(i)s_{-1}(i)|bS_bS_b\rangle \times \langle bS_bS_b|\sum_{A,i}\xi(r_{iA})l_{A,q}(i)s_{+1}(i)|aS_aS_a\rangle \quad (5)$$

$$D_{pq}^{(-1)} = -\frac{1}{S_a(2S_a-1)} \times \sum_b \Delta_b^{-1}\delta_{S_bS_a-1}\langle aS_aS_a|\sum_{A,i}\xi(r_{iA})l_{A,p}(i)s_{+1}(i)|bS_bS_b\rangle \times \langle bS_bS_b|\sum_{A,i}\xi(r_{iA})l_{A,q}(i)s_{-1}(i)|aS_aS_a\rangle \quad (6)$$

The symbols and assumptions in eqs 5 and 6 are the same as in eq 3. An important difference arises when calculating **D**-tensor contributions from excited states that are not described by a single determinant. Contributing $\Delta S = 0$ (i.e., $^4\Gamma \rightarrow {}^4\Gamma$), spin-raising $\Delta S = +1$ (i.e., $^4\Gamma \rightarrow {}^6\Gamma$), and spin-pairing $\Delta S = -1$ (i.e., $^4\Gamma \rightarrow {}^2\Gamma$ with one unpaired electron in the excited state) transitions can be described by a single determinant. Spin-lowering, $\Delta S = -1$ one-electron transitions from a $^4\Gamma$ ground state to excited states with three ($^2\Gamma$) or five ($^2\Gamma$) unpaired electrons do not possess maximal spin multiplicity and often require a multideterminant description. The wave functions for multideterminant states were approximated by generating the coupled spin-function states,[34,35] then allowing the component microstates to undergo two-electron intraconfigurational Coulomb and exchange interactions.[36−39] This method was calibrated using single-determinant excited state energy calculations. The resulting term energies varied by up to 15% from their component single determinant energies, indicating that they should be included when quantifying the $\Delta S = -1$ contributions to D.

The three contributors are summed to give the total $D_{pq}^{(\text{tot})} = D_{pq}^{(0)} + D_{pq}^{(+1)} + D_{pq}^{(-1)}$. The $\Delta S = \pm 1$ contributions are found to make significant contributions to D_{xx}, D_{yy}, and D_{zz}, with the primary contribution arising from the single-determinant spin-paired states within the t_2* set of orbitals $D_{xx}^{(-1)}(yz(+)\uparrow \rightarrow x^2{-}y^2(+)\downarrow)$ and $D_{xx}^{(-1)}(x^2{-}y^2(+)\uparrow \rightarrow yz(+)\downarrow)$. The final calculated value for D $(=D_{z'z'}^{(\text{tot})} - 1/2(D_{x'x'}^{(\text{tot})} + D_{y'y'}^{(\text{tot})}))$ was 35.5 cm^{-1} with $E/D = 0.14$ ($E/D = (D_{x'x'}^{(\text{tot})} - D_{y'y'}^{(\text{tot})})/2D$). While there is good agreement between the experimental ($D_{\text{exp}} = 38 \pm 3$ cm^{-1}) and calculated sign and magnitude of D, the calculated rhombicity was greater than experiment ($(E/D)_{\text{exp}} = \sim 0.05$). This was due to the small energy denominator for the $D_{yy}^{(+1)}(xz(+) \rightarrow z^2(+))$ and $D_{yy}^{(-1)}(xz(+) \rightarrow z^2(+))$ terms relative to the $D_{zz}^{(+1)}(x^2{-}y^2(-) \rightarrow xy(-))$ and $D_{zz}^{(-1)}(x^2{-}y^2(-) \rightarrow xy(-))$ terms and may reflect a shortcoming in the DFT-calculated wave function or the assumptions made in **D**-tensor calculation. This calculation shows that it is necessary to consider second-order $\Delta S = \pm 1$ spin−orbit mixing in order to account for this unusually large value for D. Most importantly, it identifies the origin of large ZFS as spin−orbit coupling to

---

(34) Sugano, S.; Tanabe, Y.; Kamimura, H. *Multiplets of Transition Metal Ions in Crystals*; Academic Press: New York, 1970.

(35) Zare, R. N. *Angular Momentum*; John Wiley & Sons: New York, 1988.

(36) Solomon, E. I.; Lever, A. B. P. In *Inorganic Electronic Structure and Spectroscopy*; Solomon, E. I., Lever, A. B. P., Eds.; John Wiley & Sons: New York, 1999; Vol. 1, pp 1−92.

(37) Ziegler, T.; Rauk, A.; Baerends, E. J. *Theor. Chim. Acta* **1977**, *43*, 261−271.

(38) Von Barth, U. *Phys. Rev. A* **1979**, *20*, 1693−1702.

(39) Ziegler, T. *Chem. Rev.* **1991**, *91*, 651−667.

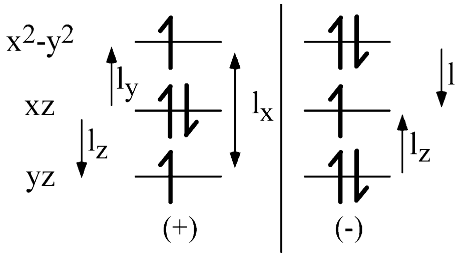

Figure 5. The t_2 (doubly occupied) and t_2* (singly occupied) set of orbitals arranged by inversion symmetry. The arrows indicate symmetry-allowed spin−orbit mixing. Single arrows correspond to $\Delta S = 0$ while the double arrow corresponds to $\Delta S = -1$ spin−orbit coupling.

low-lying $\Delta S = -1$ t_2* excited states and shows that the unique magnetic axis (z') is equivalent to the molecular x-axis, consistent with the calculated **g**-matrix.

5. Discussion

The coaxial alignment of the **g**-matrix and ZFS-tensor may appear to be coincidental as g_x is distinct due to a lack of significant $\Delta S = 0$ spin−orbit coupling into the ground state via L_x while D_{xx} is largest due to $\Delta S = -1$ spin−orbit coupling. Applying the angular momentum operator to the six t_2/t_2* orbitals generates six nonzero integrals: $\langle x^2-y^2(\pm)|l_x|yz(\pm)\rangle$, $\langle x^2-y^2(\pm)|l_y|xz(\pm)\rangle$, and $\langle xz(\pm)|l_z|yz(\pm)\rangle$.[25] Referring to Figure 5, it is apparent that the only possible $\Delta S = -1$ mixing (orbital angular momentum operator maintains the parity of a wave function) is $\langle x^2-y^2(+)|l_x|yz(+)\rangle$, indicating that the unique **D**-tensor direction is x. Similarly, the $\Delta S = 0$ mixings can only be due to l_y or l_z; from the doubly occupied $xz(+)$ orbital to the singly occupied $x^2-y^2(+)$ (i.e., l_y-coupled) and $yz(+)$ (i.e., l_z-coupled) and to the singly occupied the $xz(-)$ orbital from the doubly occupied $x^2-y^2(-)$ (l_y) and $yz(-)$ (l_z) orbitals. Hence, the EPR g-values significantly deviate from 2.0023 in the y- and z-directions, but not the x-direction. Thus, the t_2/t_2* orbital splitting which prevents l_x, $\Delta S = 0$ mixing is the same as that which makes l_x, $\Delta S = -1$ mixing large.

It is of interest to note that the axial direction of the magnetic tensors does not coincide with the unique rotation axis of the C_{2h}-symmetry Fe_2O_2 core. The C_2 axis is normal to the Fe_2O_2 plane, while the magnetically distinct direction is along the Fe−Fe vector. This inequivalence occurs as the C_{2h} symmetry group is rhombic with three unique axes and imposes no constraints upon the relationship between any molecular properties projected upon these axes. The lack of any symmetry-imposed constraints upon the relative magnitudes of the components of the **g**-matrix and **D**-tensor raises the question of why they are so strongly axial (the rhombicity (E/D) of the **D**-tensor is 0.05). This is due to the orbital occupation and ligand-field splitting of the t_2/t_2* set of orbitals which results in a specific orbital occupation pattern and permits $\Delta S = -1$ spin−orbit coupling between only one pair of orbitals in the t_2/t_2* set; $x^2-y^2(+)$ and $yz(+)$. This accounts for the large observed zero-field splitting and defines the orientation of the magnetic coordinate system relative to the molecular coordinate system. The latter is of vital importance to the assignment of the electronic spectrum as it allows the transition polarizations elucidated from VTVH MCD saturation fitting to be related to the molecular coordinate system.[12]

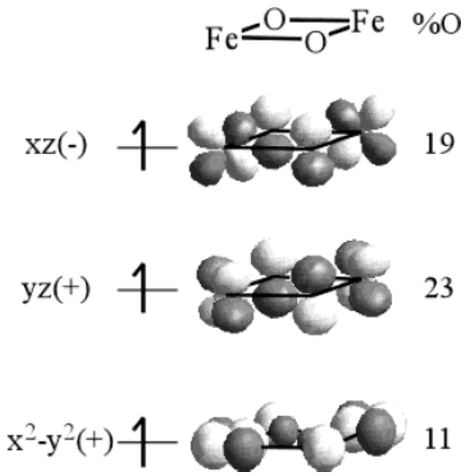

Figure 6. Qualitative representation of the Fe_2O_2 core SOMOs showing their covalency-scaled oxo contributions derived from the combination of ^{17}O superhyperfine broadening and DFT calculations.

The anisotropic ^{17}O superhyperfine broadening analysis has verified the predicted t_2/t_2* splitting in the iron d-manifold. It shows that the predominant oxo density in these orbitals is oriented perpendicular to the Fe_2O_2 plane as two ($xz(-)$ and $yz(+)$) have strong p_z contributions (Figure 6). These orbitals also constitute good superexchange pathways that allow electron density to be delocalized over the Fe_2O_2 core. We have shown that these pathways give rise to the observed valence-delocalization and $S = {}^3/_2$ ground state.[12] Additionally, determining the nature of the singly occupied molecular orbitals allows one to explore this molecule's reactivity as these orbitals are activated for hydrogen atom abstraction due to their low energy and high oxo content.[12]

Acknowledgment. The authors thank Dr. Frank Neese for helpful discussion. This work was supported by grants from the NSF Biophysics Program (9816051 to E.I.S.) and the National Institutes of Health (GM-38767 to L.Q). A.J.S. was supported by a predoctoral fellowship from the NSF.

Supporting Information Available: Coordinates of $Fe_2O_2(NH_3)_8$ DFT model and additional simulated ^{17}O EPR spectra. This material is available free of charge via the Internet at http://pubs.acs.org.

IC034170Z